Universiteit Leiden
The Netherlands

Analysis of electron donors in photosystems in oxygenic photosynthesis by photo-CIDNP MAS NMR

Najdanova, M.; Janssen, G.J.; Groot, H.J.M. de; Matysik, J.; Alia, A.

Citation
Najdanova, M., Janssen, G. J., Groot, H. J. M. de, Matysik, J., & Alia, A. (2015). Analysis of electron donors in photosystems in oxygenic photosynthesis by photo-CIDNP MAS NMR. *Journal Of Photochemistry And Photobiology B-Biology*, *152*(B), 261–271. doi:10.1016/j.jphotobiol.2015.08.001

Version: Publisher's Version
License: Licensed under Article 25fa Copyright Act/Law (Amendment Taverne)
Downloaded from: https://hdl.handle.net/1887/3175729

Note: To cite this publication please use the final published version (if applicable).

Journal of Photochemistry and Photobiology B: Biology 152 (2015) 261–271

Contents lists available at ScienceDirect

Journal of Photochemistry and Photobiology B: Biology

journal homepage: www.elsevier.com/locate/jphotobiol

Short Review

Analysis of electron donors in photosystems in oxygenic photosynthesis by photo-CIDNP MAS NMR

M. Najdanova [a], G.J. Janssen [b], H.J.M. de Groot [b], J. Matysik [a], A. Alia [b,c,*]

[a] University of Leipzig, Institute of Analytical Chemistry, Johannisallee 29, D-04103 Leipzig, Germany
[b] University of Leiden, Leiden Institute of Chemistry, Einsteinweg 55, P.O. Box 9502, 2300 RA Leiden, The Netherlands
[c] University of Leipzig, Institute of Medical Physics and Biophysics, Härtelstr. 16-18, D-04107 Leipzig, Germany

ARTICLE INFO

Article history:
Received 8 June 2015
Received in revised form 4 August 2015
Accepted 5 August 2015
Available online 7 August 2015

Keywords:
Electron donor
Photo-CIDNP
Photosynthesis
Photosystem I
Photosystem II
Redox potential
Solid-state NMR

ABSTRACT

Both photosystem I and photosystem II are considerably similar in molecular architecture but they operate at very different electrochemical potentials. The origin of the different redox properties of these RCs is not yet clear. In recent years, insight was gained into the electronic structure of photosynthetic cofactors through the application of photochemically induced dynamic nuclear polarization (photo-CIDNP) with magic-angle spinning NMR (MAS NMR). Non-Boltzmann populated nuclear spin states of the radical pair lead to strongly enhanced signal intensities that allow one to observe the solid-state photo-CIDNP effect from both photosystem I and II from isolated reaction center of spinach (*Spinacia oleracea*) and duckweed (*Spirodela oligorrhiza*) and from the intact cells of the cyanobacterium *Synechocystis* by ^{13}C and ^{15}N MAS NMR. This review provides an overview on the photo-CIDNP MAS NMR studies performed on PSI and PSII that provide important ingredients toward reconstruction of the electronic structures of the donors in PSI and PSII.

© 2015 Elsevier B.V. All rights reserved.

Contents

1. Introduction . . . 262
   1.1. Photosystem I . . . 262
   1.2. Photosystem II . . . 262
2. Photo-CIDNP MAS NMR as a spectroscopic method . . . 263
3. Photo-CIDNP MAS NMR studies on the photosynthetic reaction center . . . 264
4. Photo-CIDNP MAS NMR studies on the photosystem I (PSI) . . . 264
   4.1. Photo-CIDNP on unlabeled PSI reaction centers . . . 264
   4.2. ^{15}N photo-CIDNP reveals large flexibility of PSI in terms of electronic architecture . . . 265
   4.3. Observation of PSI photo-CIDNP directly from intact cells of Synechocystis . . . 266
5. Photo-CIDNP MAS NMR studies on the photosystem II (PSII) reaction center . . . 267
   5.1. ^{13}C- photo-CIDNP MAS NMR studies on PSII reaction centers . . . 267
   5.2. ^{15}N- photo-CIDNP MAS NMR studies on PSII reaction centers . . . 268
   5.3. The hinge model of the electron donor in PSII . . . 268
6. Magnetic field effect of the photo-CIDNP observed in photosystem I and II reaction centers . . . 268
7. Summary and outlook . . . 269
   Acknowledgements . . . 269
   References . . . 269

* Corresponding author at: University of Leipzig, Institute of Medical Physics and Biophysics, Härtelstr. 16-18, D-04107 Leipzig, Germany.
E-mail address: alia.aliamatysik@medizin.uni-leipzig.de (A. Alia).

http://dx.doi.org/10.1016/j.jphotobiol.2015.08.001
1011-1344/© 2015 Elsevier B.V. All rights reserved.

1. Introduction

Plants and algae are an integral part of our ecosystem. Plants and other photosynthetic organisms are a source of food and fibers and reduce atmospheric carbon dioxide while supplying oxygen to the atmosphere. They can be considered as the heart of life on earth to which animals and humans own their existence. By increasing our understanding about photosynthesis, we ultimately aim to find sustainable and safe solutions for man's increasing demand for energy. Solutions based on solar energy avoid both the excessive use of fossil fuels and subsequent environmental problems and the danger involved with nuclear power plants.

Natural photosynthesis is the process of capturing sunlight and its conversion into chemical energy bound in organic molecules. In plants and cyanobacteria, photosynthesis is driven by two efficient electron pumps embedded in the thylakoid membrane, Photosystem I (PSI) and Photosystem II (PSII) [1,2]. These photosystems represent large membrane pigment–protein complexes, mutually connected through an electron transport chain. The general molecular architecture of both photosystems appears to be considerably similar. In both photosystems, the light-dependent reaction is initiated upon absorption of sunlight, which results in photo-oxidation of the chlorophyll *a* (Chl *a*) molecules of the primary electron donors (P). The photochemically transferred electron moves along a series of cofactors forming an electron transfer chain, thus generating a charge gradient across the membrane.

1.1. Photosystem I

The photosystem I core complex in higher plants is made up of approximately 12 different subunits, which are bound to 4 light-harvesting proteins (LHCI antenna complex) [3,4]. The reaction center of PSI comprises of two nearly symmetric branches of cofactors, which contain six chlorophyll molecules and two phylloquinones, arranged in two chains along a pseudo twofold (pseudo-C_2) symmetry axis. Furthermore, PSI contains three iron sulfur clusters (F_X, F_A, F_B) as terminal intrinsic electron acceptors [5,6] (Fig. 1A). The two branches of cofactors, branches A and B, have been named according to their association with the respective protein subunits PsaA and PsaB, which accommodate the electron transport chain cofactors. The primary electron donor P700 is a heterodimer consisting of one chlorophyll *a* (Chl *a*, P_B) and one chlorophyll *a*′ (Chl *a*′, P_A) which is the 13^2-epimer of Chl *a*. While P_A forms hydrogen bonds to its protein environment, no hydrogen bonds are found on the P_B side [7–9]. EPR studies showed most of the positive charge to be localized on the Chl *a* (the P_B donor) molecule [9–12], however a consensus about the extent of asymmetry has not yet been reached [13,14]. The photochemical charge separation, occurring from the lowest excited singlet state of P700, leads to the radical-pair formation. The electron transfer is linked to both charge and spin transfer. Recent optical spectroscopic studies imply the possibility for an asymmetric primary charge separation [10,15–17], pointing out the accessory chlorophyll A_{-1} as the primary electron donor which in turn forms a radical pair $A_{-1}^{\cdot+}$ $A_0^{\cdot-}$ with a lifetime of a few radical pair $P700^{\cdot+}$ $A_0^{\cdot-}$. These findings repeal the proposal of the P700 heterodimer structural asymmetry as a conclusive argument against a bidirectional electron transfer observed in PSI. In PSI both electron pathways can be active, a phenomenon generally referred to as bidirectional electron transfer (for a review, see [14]). The electron transfer through accessory chlorophylls develops a comparable reduction potential in both A_0 upstream chlorophylls of the two branches. Consequently the phylloquinones (A_{1A}, A_{1B}) are reduced, which function independently from each other and transport electrons to the Fx iron cluster within 200 ns [18]. The fact that both phylloquinones operate independently and act as electron transfer intermediates, is a possible hint to bidirectional or symmetrical electron transfer in PSI. The overall lifetime of the $P700^{\cdot+}$ radical cation has reported to be in the order of tens of milliseconds [19,20]. Mutagenesis studies [21–23], as well as optical and transient EPR studies suggest distinct electron transfer efficiency between both branches which are organism dependent. For example, the electron transfer is reported to be biased toward the A-branch in both cyanobacteria and green algae. However, the bias is stronger in the case of cyanobacteria [10,24–27]. Although the knowledge of the structural organization of the cofactors is continuously expanding, the question of the directionality of the electron transfer among different species and the precise molecular mechanism of charge separation are not fully understood.

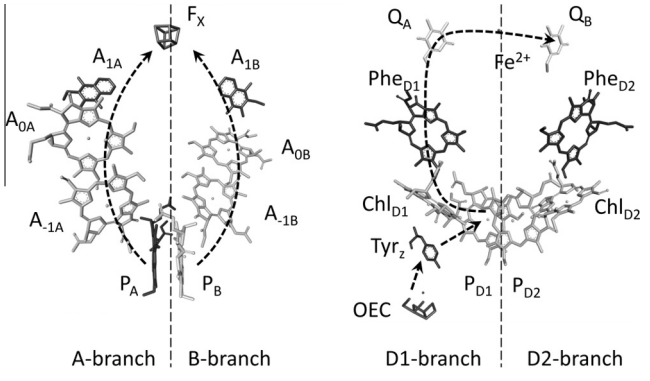

Fig. 1. (A) Spatial arrangement of the PSI RC cofactors based on the X-ray crystal structure of cyanobacterial PSI of *Synechococcus elongatus* [8]. (B) Spatial arrangement of PSII RC cofactors of the core complex of *Thermosynechococcus elongatus* [31]. In both RCs, the cofactors are nearly arranged in a C_2 symmetry perpendicular to the membrane plane as indicated by the axes. Structures are visualized using Accelrys Discovery Studio (Accelrys Software Inc., San Diego).

1.2. Photosystem II

PSII is a multisubunit membrane protein complex. Recently a high resolution X-ray structure of PSII (Fig. 1B) from the cyanobacterium *Thermococcus vulcanus* was resolved down to 1.9 Å resolution [28]. The PSII core complex consists of more than 20 distinct subunits and various functionally significant cofactors [29]. At the heart of this multiprotein complex is the PSII reaction center (RC), comprising the D1 and D2 polypeptides that bind the cofactors involved in the primary electron transfer process. These cofactors include six chlorophyll *a* molecules, from which four are believed to be active in the initial charge separation. In addition two pheophytins, two β-carotenes, two plastoquinones and an iron atom are part of the PSII RC. The central electron donor cofactor pair, P680, is structurally analogous to the 'special pair' in bacterial RC of *Rhodobacter sphaeroides* (*R. sphaeroides*) and P700 in PSI. It comprises of two Chl *a* molecules, denoted as P_{D1} and P_{D2} [30,31]. The cofactors in PSII RCs are arranged in two branches perpendicular to the plane of the membrane, having almost a C_2 symmetry. Despite the high symmetry, only one branch is active in the electron transfer from the electron donor to the plastoquinones [35]. On illumination P680 is initially brought into its first electronically excited singlet state and donates the energized electron within a few picoseconds to a pheophytin (Phe) molecule to form the radical pair state $P_{680}^{+}Phe^{\cdot-}$. There are a number of studies suggesting that the primary charge separation in PS II could be between the accessory chlorophyll and the pheophytin [15–17,32–34]. From $Phe^{\cdot-}$ the electron is transported to a bound plastoquinone molecule (Q_A) within 300 ps. P_{680}^{+} is reduced within nano- to microseconds by a redox active tyrosine (Y_Z) at position

161 of the D1 protein. Y_Z is then reduced by a tetra-manganese cluster, which stores the oxidation equivalents needed for oxidizing water to molecular oxygen. PSII can generate a potential up to 1.2 V [36,37] which is much higher than the potential of 0.5 V observed for the special pair electron donor P840 in the bacterial RC [38]. This makes the oxidized electron donor of PSII, $P680^{\cdot+}$, the strongest oxidizing agent known in living nature.

Despite the similarity in molecular architecture, the electric midpoint potential of PSII and PSI is extremely different. The antagonistic electrochemical properties of these reaction centers enable an exceptional cooperation. The oxidized state of PSII forms a uniquely strong oxidizing redox potential that is sufficient for splitting water. The photochemical excited state of PSI, with its strong reductive power, supplies the electrons for the reduction of atmospheric carbon dioxide. The origin of the very different redox properties of both RCs is not yet fully understood. In bacterial reaction centers invaluable insight into the orbital architecture of the electron donor has been provided by photo-CIDNP MAS NMR [39,40]. In this review, we will summarize recent photo-CIDNP MAS NMR studies on PSI and PSII that allow the reconstruction of the electronic structures of the donors in PSI and PSII.

2. Photo-CIDNP MAS NMR as a spectroscopic method

Photochemically induced dynamic nuclear polarization (photo-CIDNP) magic-angle spinning (MAS) NMR is an analytical method for the study of spin-correlated radical pairs. It is particularly attractive because it combines the high sensitivity and selectivity of the solid-state photo-CIDNP effect with the versatility of MAS NMR techniques. Conveniently, this hyperpolarization effect can be obtained simply by irradiating with light.

Enhancement of NMR signal intensities by CIDNP has been first observed by liquid state NMR in 1967. The discovery was made independently by two research teams, namely Bargon and Fischer [41], and Ward and Lawler [42]. Soon after this discovery, the classical "radical pair mechanism" (RPM) was proposed [43,44].

The classical RPM acts as a spin-sorting mechanism at high field during the inter-system crossing (ISC) process, thus separating the nuclear spin polarization into two groups of signals having the same integral but opposite sign [41,43]. If both products have the same chemical fate, their signals will cancel each other, and no enhancement will be observed. In liquid state, singlet radical pairs can recombine but triplet radical pairs diffuse apart. In photosynthetic RCs, the RPM can be observed in time-resolved laser-flash experiments as an early phase, remaining until also the triplet branch population decays to the ground state [39]. The RPM is, however, not visible in the solid state under continuous illumination since it relies on the molecular diffusion, hence it cannot be considered as a plausible explanation of the solid-state photo-CIDNP effect observed in frozen RCs under steady-state illumination [45].

The solid-state photo-CIDNP effect has been first observed in 1994 by Zysmilich and McDermott [46,47], on a frozen quinone-blocked bacterial RC by ^{15}N MAS NMR under continuous illumination with white light. Due to the transient non-Boltzmann distribution of the population of nuclear spin states in rigid samples upon photo-reaction, a strong signal enhancement has been observed in several different RC species by ^{13}C and ^{15}N MAS NMR [13,48–56]. The representative solid-state photo-CIDNP spectra in RCs of *R. sphaeroides* WT and R26 are shown in Fig. 2A.

The mechanism by which the photo-CIDNP polarization is born in quinone-blocked bacterial RCs of *R. sphaeroides* at high magnetic fields and under continuous illumination is explained by up to three mechanisms running in parallel and requiring anisotropic hyperfine couplings [45,47] (Fig. 2B). Common features of all three mechanisms is a net total nuclear spin population after summing over both decay branches. This results in a strong steady-state nuclear polarization readily detectable by NMR after decay of the radical pair.

Upon formation of the photosynthetic spin-correlated radical pair under illumination, a pure singlet state (S) is established having a high mutual electron spin order and allowing for a zero-quantum coherence between the eigenstates of the radical pair [57]. This high electron correlation can lead to high polarization of neighboring nuclei via two coherent solid-state mechanisms:

1. *Electron–electron–nuclear* three-spin mixing (TSM). The coherent spin evolution within the spin correlated radical pair state during inter-system crossing (ISC), results in a break of balance of the two radical pair decay channels, which is controlled by the sign of the anisotropic electron–electron and the electron–nuclear pseudosecular hyperfine (hf) interactions [58,59]. Limiting factor for the maximal state mixing is the attainment of the double matching condition $2|\Delta\Omega| = 2|\omega_I| = |A|$. This implies that the difference between the electron Zeeman frequencies ($\Delta\Omega$) needs to match the nuclear Zeeman frequency (ω_I) and they both need to match the diagonal (secular) part of the hyperfine interaction (A). Through the three energy level matching, the electron ZQC is passed over to the nuclei as polarization. Since the pseudosecular part of the hyperfine interaction is the main driving force of this mechanism, it cancels out when the hf anisotropy is averaged. Therefore, TSM polarization is not observable in the liquid state.
2. *Differential decay* (DD). The lifetimes of the singlet (S) and the triplet (T_0) states of the radical pair differ. This difference breaks the balance between the two decay channels. Due to the two spin states of the radical pair, different portions of polarization are transferred to the nuclei, causing further imbalance between the fraction of nuclei having a spin-up and the fraction of nuclei having a spin-down state. For the DD mechanism, a single energy level matching condition $2|\omega_I| = |A|$ is required. The performance of the mechanism is directly dependent on the difference of S and T_0 radical pair lifetimes, which need to be of the magnitude of the inverse hf interaction. Since again the anisotropic part of the hyperfine coupling is required, this mechanism, too, is not observable in the liquid state [40,45,60].

In RCs of *R. sphaeroides* WT, according to the theory [45], the TSM leads to emissive (negative) intensities, while the DD causes enhanced absorptive (positive) signals. Since the entire envelope is emissive, the TSM overrules the DD [48]. The magnetic field interacts with both electron and nuclear spin magnetic moments causing the dependence of $\Delta\Omega$ and ω_I on the magnetic field strength. On the other hand, hyperfine couplings are not field dependent. Therefore, both TSM and DD have their field dependence and maxima according to their specific matching conditions. Some RCs, such as the carotenoid-depleted R26 mutant of *R. sphaeroides*, have a long-lived triplet state of the donor cofactor (^3P), which allows for the occurrence of a third mechanism found in the solid-state photo-CIDNP:

3. *Differential relaxation* (DR). This mechanism, occurring in solid and liquid state, follows the sign rules of the RPM [61]. It is also known as 'cyclic reactions'. Although the polarization generated in cyclic reactions is expected to be completely canceled out due to the different longitudinal relaxation rates of the nuclear spins in both branches, the polarization is partially preserved

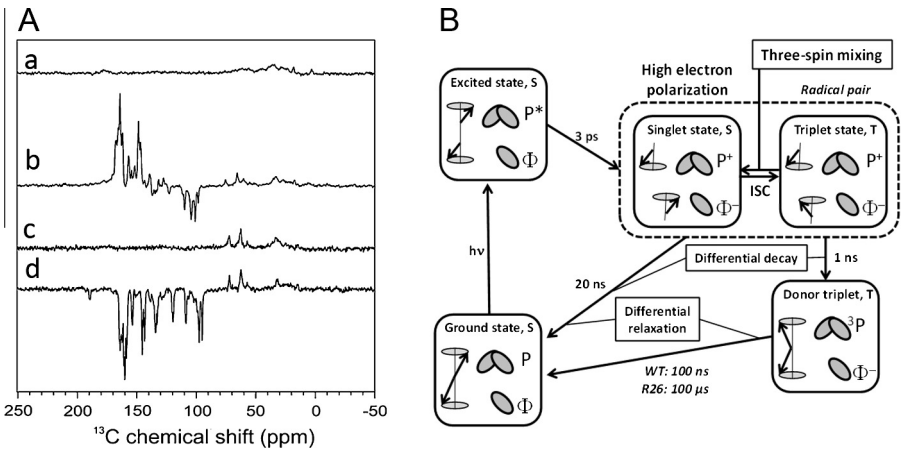

Fig. 2. ^{13}C MAS NMR photo-CIDNP spectrum of isolated RC from *R. sphaeroides* R26 (a, b) and wildtype (WT) (c, d). The spectra a and c are obtained under dark conditions, whereas spectra b and d are recorded under continuous illumination with white light. All spectra were obtained at a temperature of 230 K, a magnetic field of 4.7 T and a cycle delay of 4 s (Reprinted, with permission, from Prakash et al. [48]). © The American Chemical Society. (B) Mechanism of the photo-CIDNP buildup in natural RCs of *R. sphaeroides* WT and R26, established for high magnetic field conditions. Upon illumination, the photochemically excited donor special pair (P^*) transfers an electron to the primary acceptor Φ, bacteriopheophytin. A radical pair ($P^{+\cdot}\,\Phi^{-\cdot}$) initially in a singlet is born carrying high electron spin order. The radical pair oscillates between its singlet and triplet state T_0. During the intersystem crossing process (ISC), polarization buildup from the correlated electron pair to the surrounding nuclei occurs via the three-spin-mixing (TSM). Back electron transfer from the radical pair singlet state results in an electronic ground state, while a back electron transfer from the radical pair triplet state, leads to a donor triplet state (^{3}P). The differential decay (DD) mechanism underlines the buildup of a *net* photo-CIDNP due to the different contributions of the two spin states of the spin-correlated radical pair on the spin evolution. In RCs having a long-lived donor triplet state, ^{3}P, as in the case of R26, differential relaxation (DR) becomes significant, due to pronounced nuclear spin relaxation on the triplet branch, resulting in partial cancellation of nuclear polarization in the triplet branch.

[43,62,63]. Consequently, the DR is strongly dependent on the enhanced nuclear relaxation in the triplet branch originating from the fluctuating hyperfine interactions between the nuclei and the donor triplet state (^{3}P). From this aspect, it can be considered that the relative line intensities also maintain the information of the local spin density distribution within the donor triplet state [40,48].

The two pure solid-state mechanisms, TSM and DD, which transfer the polarization from the electron to the nuclear order on *nanosecond time* scale, occur in PSI. The DR mechanism requires a long lifetime of the donor triplet state and does not contribute to polarization build up in PSI. Moreover, all of the previously discussed mechanisms allow for a correlation of NMR signal intensity and local electron spin density in either the radical pair state (TSM, DD) or the donor triplet state (DR) [40]. In addition, the enhanced signals allow for the selective observation of chemical shifts related to the electronic ground-state structure. Hence, photo-CIDNP MAS NMR is a versatile analytical tool for the analysis of transient spin-correlated radical pairs permitting an atomic-level "view" on the electronic structure of the RC apparatus [64].

Although the parameter window allowing the solid-state photo-CIDNP effect is narrow [45,52,65], the effect has been observed in all RCs investigated up to now [60]. Therefore, it has been inferred that the solid-state photo-CIDNP effect is an intrinsic property of natural photosynthetic RCs that is evolutionary conserved [66]. This would imply functional relevance under natural conditions, such as the earth's magnetic field [67] and liquid-state membranes [68].

3. Photo-CIDNP MAS NMR studies on the photosynthetic reaction center

In the meanwhile, following the observation of the solid-state photo-CIDNP in purple bacterial reaction centers, the same effect is observed in other natural photosynthetic systems, such as frozen samples of heliobacteria [40,52,69], green sulfur bacteria *Chlorobium tepidum* [51] as well as in isolated RC of spinach (*Spinacia oleracea*) [13,51,53,54,70] and duckweed (*Spirodela oligorrhiza*) and in whole cells of cyanobacterium (*Synechocystis* sp. PCC 6803 strain) [55,56]. In the following section we will focus on photo-CIDNP MAS NMR studies on PSI and PSII which lead to an insight into the electronic structure of the primary donor $P700^*$ and $P680^{+\cdot}$.

4. Photo-CIDNP MAS NMR studies on the photosystem I (PSI)

4.1. Photo-CIDNP on unlabeled PSI reaction centers

The first observation of the photo-CIDNP in PSI has been reported in isolated PSI from spinach [13]. Two types of PSI preparations have been used: (i) an isolated PSI complex containing ~110 Chl/P700 (the so-called PSI-110 preparation), having reduced terminal ferredoxin acceptors, and (ii) a CPI RC complex, having PSI particles with ~40 Chl/P700 and lacking the terminal ferredoxin acceptors. Remarkable enhancement of NMR signals from the active site of PSI has been observed in both preparations without any isotope enrichment. Interestingly, light induced photo-CIDNP signals originating from the light-induced radical pair cofactors were all emissive and appeared exclusively in the aromatic region [13,70] (Fig. 3A).

Most of the light induced signals from PSI appeared in the region between 100 and 200 ppm. A total of 12 isotropic chemical shifts, i.e., centerbands independent of the MAS rotational frequency [13], have been resolved from the spectrum. These signals have been assigned to 17 carbon atoms belonging to a single Chl *a* molecule, probably the P_B cofactor of the P700 electron donor (Table 1). The strongest signal enhancement was detected in the aromatic region between 120 and 170 ppm. Signals coming from aliphatic carbons or the methine carbons C-5 and C-20 were not present in the spectrum (Fig. 3A). In general, the linewidth of the NMR signals is related to the internal order and dynamics. The linewidth observed for light-induced signals in PSI was significantly narrow (60–65 Hz), which is a convincing indicator for a high overall rigidity and order of the donor site, experiencing low electron transfer reorganization energies.

The origin of the photo-CIDNP enhancement was proposed to be due to the formation of the more stable radical pair

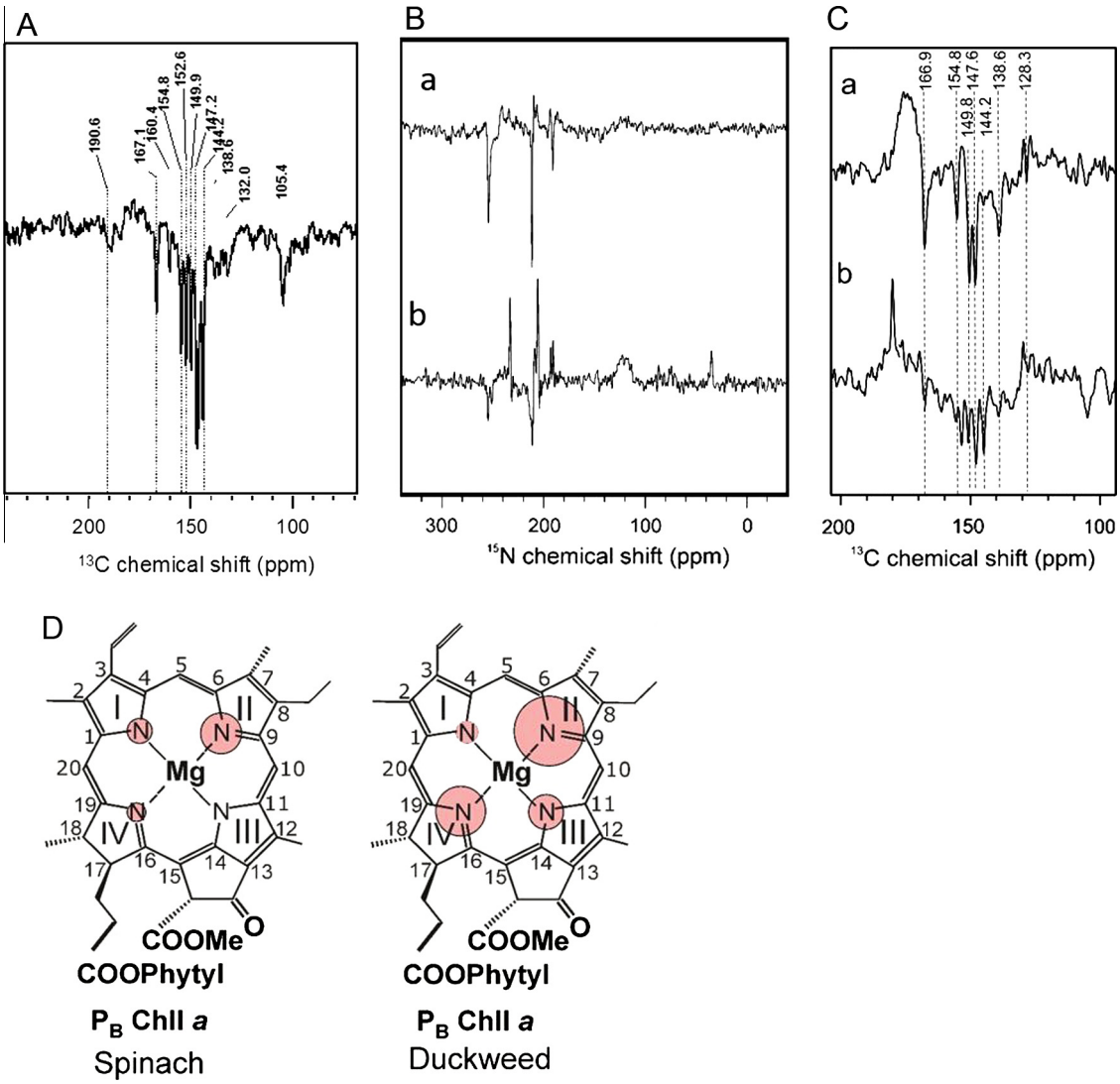

Fig. 3. (A) ^{13}C MAS NMR spectra of PSI-110 particles obtained at a temperature of 223 K, a magnetic field strength of 9.6 T and a MAS frequency of 9 kHz under continuous illumination with white light; (B) ^{15}N photo-CIDNP MAS NMR spectra of PSI-110 particles of duckweed (A) and spinach (B) under continuous illumination at a temperature of 240 K, a magnetic field strength of 9.4 T, a MAS frequency of 8 kHz and a cycle delay of 4 s (Reprinted, with permission, from Janssen et al. [56]). © Springer; (C) ^{13}C MAS NMR spectra of: fresh [4-^{13}C]-ALA-labeled *Synechocystis* cells (a) and (b) Isolated PSI (PSI-110 preparation from spinach without isotope enrichment). All spectra have been obtained under continuous illumination by white light at a temperature of 235 K, a MAS frequency of 8 kHz and a magnetic field strength of 4.7 T. (Reprinted, with permission, from Janssen et al. [55]). © Springer; (D) ESD patterns of the primary donor of the B branch (P_B) of PSI of spinach and duckweed obtained on basis of ^{15}N photo-CIDNP intensities. Modified from Janssen et al. [56]) © Springer.

$P700^{+}\cdot A_0^{-}\cdot$, born in a pure electronic singlet state which is converted into a net nuclear polarization via the TSM and DD mechanism [45,58,59]. As discussed by Alia et al., due to the strong electronic coupling in the radical pair formed upon illumination, the birth of triplet states was not expected and therefore no DR contribution was suggested. The DFT calculations also suggested a predominance of the TSM over the DD mechanism in PSI.

The photo-CIDNP spectra of both PSI samples reveal a single Chl *a* set of resonances (Table 1). Since in PSI both the donor and the primary acceptor are Chl *a* cofactors, the possibility that the spectrum contains signals from both the donor and acceptor cofactors could not be excluded on the basis of only chemical shifts. However, the DFT calculations suggested that the majority of the light-induced signals are arising from the donor rather than the acceptor [13], thus implying that the photo-CIDNP signals mainly originate from a single Chl *a*, assumable P_B.

4.2. ^{15}N photo-CIDNP reveals large flexibility of PSI in terms of electronic architecture

To obtain deeper inside into the electronic structure of PSI and to accurately map the electron spin density in active cofactors of PSI, solid-state photo-CIDNP was combined with ^{15}N isotope labeling of PSI. In order to study the rigidity and flexibility of the electronic architecture of PSI in different organism, the data was obtained from two different PSI proteins, one from ^{15}N labeled spinach [54] and other from the ^{15}N labeled aquatic plant duckweed (*S. oligorrhiza*) [56]. If the electron transfer chain in PSI is bidirectional, a maximum of sixteen nitrogen atoms can occur in the ^{15}N photo-CIDNP MAS NMR spectrum, originating from up to three Chl *a* cofactors and the single Chl *a*′ cofactor. The photo-CIDNP spectra from duckweed showed a maximum of 11 light-induced signals [56], whereas in spinach only 8 signals were observed [70] (Fig. 3B) (Table 2). The chemical shift region characteristic for the N-II nitrogen of Chl *a* reveals three signals suggesting that

Table 1
Summary of ^{13}C chemical shifts assignment of the photo-CIDNP signals from PSI and PSII from Spinach and *Synechocystis* sp. PCC8803 obtained at 4.7 T.

Chl *a*		Assign. atom	PSII	PSI	PSI + PSII (*Synechocystis*)
σ_{liq}[a]	σ_{SS}[b]		σ[c]	σ[d]	σ[e]
Chemical shifts					
189.3	190.6	13^1		~191 E	
172.7	175.3	17^3			
171.0	171.2	13^3			
		?	177.2 A		
167.4	170.0	19	166.8 A	167.1 E	166.9 E
161.4	162.0	14	162.2 A	160.4 E	
		?	160.7 A		
		?	157.4 A		
154.0	155.9	1	156.0 A	154.8 E	154.8 E
155.8	154.4	6	154.3 A		149.8 E
151.4	154.0	16	151.6 A	152.6 E	
148.0	150.7	4	149.2 A	149.9 E	
147.7	147.2	11	147.7 A	147.2 E	147.6 E
146.1	147.2	9			
144.1	146.2	8	146.0 A	144.2 E	144.2 E
		?	142.5 E		138.6 E
		?	139.8 E		
139.0	137.0	3	137.4 A	138.6 E	
135.5	136.1	2	136.0 A	~136 E	
134.2	134.0	12	133.9 A	~132 E	
134.0	133.4	7	~132 A		
131.5	126.2	13			128.3 E
		?	129.2 E		
131.5	126.2	3^1	~125 A		
118.9	113.4	3^2			
107.1	108.2	10	106.9 E	105.4 E	~104.5 E
106.2	102.8	15	104.7 E		
100.0	98.1	5	97.9 E		
92.8	93.3	20	92.2 E		
51.4		17			53.9

Abbreviations: σ = chemical shift, A = absorptive signal, E = emissive signal, ss = solid state NMR, liq = liquid state NMR, ? = unknown peak.
[a] Bargon [41]; Data obtained from solid aggregates of Chl *a*.
[b] Alia et al. [13]; Data obtained from isolated PSI particles from spinach.
[c] Diller et al. [70]; Data obtained from D_1D_2 particles of spinach.
[d] Janssen et al. [55]; Data obtained from living *Synechocystis* cells containing both PSI and PSII.

Table 2
^{15}N chemical shifts of the photo-CIDNP signals observed in PSI and PSII from spinach and duckweed.

Assignment		Solution data	PSI spinach	PSII spinach	PSI duckweed
Cofactor	Atom	σ_{liq}[A]	σ_{solid}[A,a]	σ_{solid}[A,a]	σ_{solid}[A,b]
Chl *a*	N-I	186.0	**186.2 (e)**		**186.3 (a)**
			190.9 (a)		188.6 (a)
	N-II	206.5	206.1 (a)	211.5 (e)	206.3 (a)
					210.0 (a)
			211.5 (e)		**211.4 (e)**
					191.0 (e)
	N-III	189.4	193.2 (a)	195.3 (e)	193.3 (a)
	N-IV	247.0	233.3 (a)	247.6 (e)	242.3 (a)
			250.3 (e)		247.5 (e)
					253.9 (e)
			254.9 (e)		**254.3 (e)**
Phe *a*	N-I	125.5	–		
	N-II	241.5	–		
	N-III	133.9	–	138.3 (e)	
	N-IV	295.8	–	295.0 (e)	

All shifts are referenced to liquid ammonia with use of an external standard of solid $^{15}NH_4NO_3$ (d = 23.5).
Bold printed shifts are assigned to the primary Chl *a* donor of the B-branch (P_B).
a Absorptive (positive), e emissive (negative).
[A] Chemical shift in ppm. Measured in $CDCl_3$ [62].
[a] Chemical shift in ppm [45,54].
[b] Chemical shift in ppm [56].

both electron transport braches might be active in PSI of duckweed. Direct comparison of the signal intensities in both plant systems unravels some obvious differences. The signal of N-I of P_B (186.3 ppm) is positive in duckweed but negative in spinach (Fig. 3B) and the relative signal intensity of the P_B cofactor components were more pronounced in duckweed compared to spinach. In both systems, experiments with a very short cycle delay suggested that the emissive signals originate from a very rigid donor [54]. In general, the narrow linewidths of the photo-CIDNP signals from PSI indicated that the donor is well-ordered [13] as was also observed in the special pair of *R. sphaeroides* [71].

Based on the intensities of the observed ^{15}N photo-CIDNP signals, the electron spin density (ESD) distribution was constructed for the P_B cofactor of PSI (Fig. 3D). Comparison of the ESD map of the P_B cofactor of PSI from duckweed and spinach show that both in duckweed and in spinach most ESD is located on the ring II nitrogen and little ESD is located on ring I, which is in line with the ESD distribution observed for free Chl *a* in solution. A prominent difference is that the signal assigned to the ring I nitrogen of P_B of spinach (at 186.2 ppm) is emissive in nature while in duckweed it is observed as an absorptive signal at almost the exact chemical shift (186.3 ppm). Furthermore, changes in the intensity pattern suggest fundamental differences in the radical pairs in both plant systems. Therefore one might assume that this difference is caused by another balance of the enhancement mechanisms. That would imply that parameters ruling the dynamics or architecture of the radical pair are different. The differences in the electronic architecture may be related to different distances between donor and acceptor leading to other coupling parameters.

The field dependence of the solid-state photo-CIDNP effect in PSI has been analyzed using both ^{13}C as well as ^{15}N photo-CIDNP MAS NMR studies. It was shown that the light-induced signals of PSI increase in intensity with increasing magnetic field strength from 2.4 T to 9.4 T. The maximum is at about 9.4 T and then declines. Interestingly, the ratio between absorptive and emissive signals also seems to be dependent of the magnetic field strength [54,56]. Despite differences in the intensity pattern between photo-CIDNP of PSI from duckweed and spinach, the field dependence of the solid-state photo-CIDNP effect appeared to be similar in the two systems [56].

4.3. Observation of PSI photo-CIDNP directly from intact cells of *Synechocystis*

Previous studies in *Rhodobacter* (*R.*) *sphaeroides* as well as in *Heliobacteria* have shown that the solid-state photo-CIDNP effect can be observed not only on isolated RCs but also in larger systems such as photosynthetic membranes and even whole cells [40,52,72]. This has become possible due to selective ^{15}N and/or ^{13}C isotope labeling in combination with photo-CIDNP MAS NMR.

To observe photo-CIDNP from PSI from intact cells of *Synechocystis*, selective ^{13}C isotope labeling has been successfully achieved by Janssen et al. [55]. The *Synechocystis* sp. 6803 strain was specifically ^{13}C labeled at different carbon positions of the chlorophyll cofactors by feeding them with ^{13}C labeled precursor of chlorophylls ([4-^{13}C]-δ-aminolevulenic acid, [4-^{13}C] ALA). This allowed to observe first photo-CIDNP from whole cells of *Synechocystis* [50] (Fig. 3C). Under constant illumination, the characteristic emissive signal profile of PSI photo-CIDNP in the region between 120 and 180 ppm was observed from intact *Synechocystis cells*. The direct comparison of photo-CIDNP spectra from entire cells of *Synechocystis* with that of the isolated PSI RCs of spinach shows many similarities, regardless the difference in sample preparation. Even though spinach and *Synechocystis* belong to different phylogenic domains, a high degree of structural similarity can be concluded from the closely matching photo-CIDNP

chemical shifts of both systems. In addition to the emissive photo-CIDNP signals, weak absorptive signals were also observed that presumably originate from PSII (Fig. 3C). This can be understood since *Synechocystis* cells contain both photosystems, PSI and PS II. Rögner et al. [73] reported the PSI as the ascendant photosystem in *Synechocystis*, having a PSI/PSII ratio of 9:1, thus the dominance of the emissive PSI signals over the absorptive PSII is reasonable. Table 1 summarizes the experimentally observed chemical shifts correlated to literature values of light-induced signals from isolated PSI and Chl *a* aggregates [13,70]. As discussed by Matysik et al. and Janssen et al. [55,60], the electronic properties of the photosynthetic micro-factory seem to be relatively stable upon isolation from the natural thylakoid environment.

5. Photo-CIDNP MAS NMR studies on the photosystem II (PSII) reaction center

The solid-state photo-CIDNP effect has also been detected in the PSII systems of spinach (*S. oleracea*) [13,51–54,70], duckweed (*S. oligorrhiza*) and in a cyanobacterium *Synechocystis* (sp. PCC 6803 strain) [55,56]. In this section, we will review the ^{13}C- as well as ^{15}N- photo-CIDNP MAS NMR studies on PSII reaction centers from two different plant sources. In addition, the hinge model of the electron donor in PSII for explaining its high redox properties will be discussed. Finally, the peculiarities of the photo-CIDNP effect in terms of magnetic field dependence will be compared between PSI and PSII reaction centers.

5.1. ^{13}C- photo-CIDNP MAS NMR studies on PSII reaction centers

Matysik et al. [51] reported the first observation of the photo-CIDNP signals from the PSII RC (D_1D_2cytb559) of spinach investigated by ^{13}C photo-CIDNP MAS NMR without isotope enrichment. The majority of the light induced signals were positive, except for the emissive signal that appeared at a chemical shift of 104.6 ppm (Fig. 4A). These light-enhanced NMR signals provided information on the electronic structure of the electron donor and on the p_z spin density pattern in its oxidized form. Most centerband signals were credited to a single Chl *a* cofactor that has less interaction with other pigments. Interestingly, a pronounced asymmetry of the electronic spin density distribution on that Chl *a* cofactor was observed. The spin density appears remarkably shifted toward ring III as compared to monomeric Chl *a* radical cations in solution,

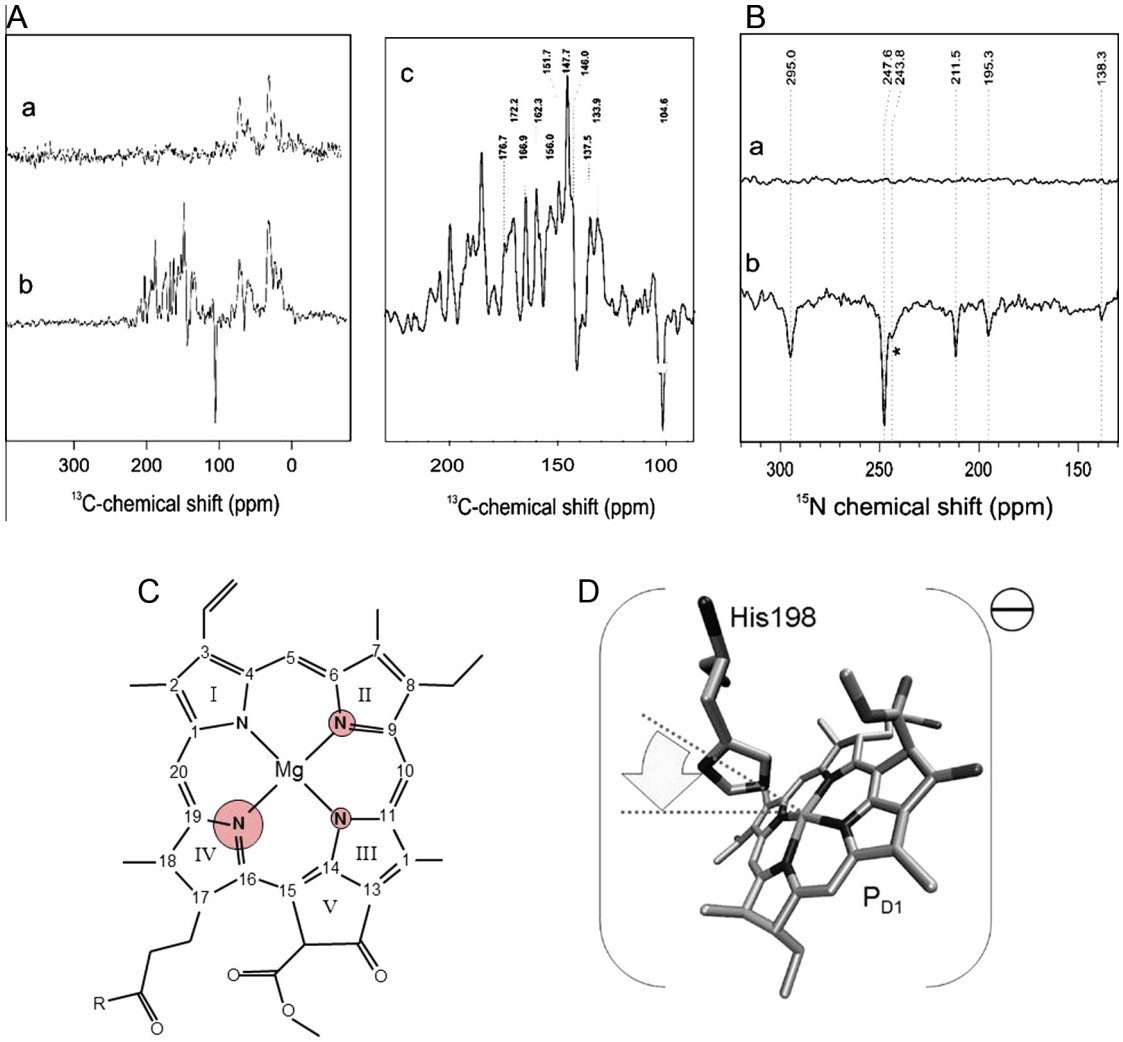

Fig. 4. (A) ^{13}C MAS NMR spectra of RCs of PSII (D1D2 preparation from spinach without isotope enrichment) in the dark (a) and under continuous illumination with white light (b, c); (B) ^{15}N MAS NMR spectra of PSII RC (D1D2 preparation from uniformly ^{15}N labeled spinach) in the dark (a) and under continuous illumination with white light (b); (C) Electron spin density pattern obtained on basis from ^{15}N photo-CIDNP intensities. The size of the circle refers to the relative signal intensity; (D) Representation of the 'hinge model' for the PSII electron donor. As a result of a tilt over the axial histidine in the direction toward pyrrole ring IV (arrow), a reversed electron spin density pattern occurs on the macrocycle and spin density is shared with the aromatic amino acid. Modified from Matysik et al. [48] and Diller et al. [54].

whereas the region of highest spin density is around ring II [12]. The radical cation electronic structure in PSII was found to be different from that in the bacterial RC, where a symmetric spin density distribution over the entire bacteriochlorophyll macrocycle was observed. Matysik et al. [53] proposed that a local electrostatic field close to ring III can polarize the electronic charge and associated spin density and may be responsible for the increase in the redox potential. The generation of such electrostatic field close to ring III could be produced, *e.g.*, by protonation of the keto group of ring V.

In a later study, Diller et al. [70] improved the ^{13}C photo-CIDNP NMR signals from the PSII RC (D_1D_2Cytb559) of spinach significantly, resulting in 23 well resolved light-induced centerband signals. The majority of the signals have been unequivocally assigned to a single Chl *a* molecule (Table 1). Diller et al. also reported the detection of four distinct methine carbon signals between 92 and 107 ppm. Two additional resonances at 157.4 and 160.7 ppm having a positive sign were tentatively assigned to the Phe *a* acceptor. The chemical shifts and photo-CIDNP intensities allowed the reconstruction of local electron spin densities on the oxidized monomeric donor. It was confirmed that the electron spin density distribution on the donor chlorophyll is highly asymmetric with a maximal electron spin density shift toward ring III/V in the donor. Diller et al. [70] also compared ^{13}C photo-CIDNP MAS NMR data of PSII to data of PSI. The comparison reveals that the electronic structure of the radical cation of P700 appears to be a Chl *a* cofactor that is essentially undisturbed, while the donor in PSII is a Chl *a* cofactor with strong matrix interaction. An electrostatic field pulling the charge toward the C-13^1 carbonyl of the Chl *a* macrocycle, stabilizing the frontier orbitals and increasing the redox force for P680 was proposed. Such an electrostatic field might be caused by hydrogen bonding, chemical modifications or transient mesoscopic changes. In the ^{13}C photo-CIDNP MAS NMR spectrum from PSII RC, two broad emissive signals at 129.2 ppm and 140–142.5 ppm that were difficult to reconcile with a Chl *a* molecule, match rather well with the carbon resonances of amino acids from the matrix. It was proposed that electron spin density is also located on aromatic amino acid of the surrounding matrix that may be involved in tuning the redox properties of the donor.

5.2. ^{15}N- photo-CIDNP MAS NMR studies on PSII reaction centers

Further insight into matrix involvement and its role in tuning the redox properties of P680 were obtained from ^{15}N photo-CIDNP studies of Diller et al. [54]. As compared to ^{13}C photo-CIDNP spectra from natural abundance PSII RC, the ^{15}N photo-CIDNP MAS NMR data from isotope labeled PSII RCs were less complicated. The spectra could be interpreted straightforwardly, as each ^{15}N signal corresponds to one of the four pyrrole nitrogens of the cofactors forming the radical pair. ^{15}N photo-CIDNP MAS NMR data of uniformly ^{15}N labeled plant PSII RCs of spinach show several emissive signals and their pattern indicated that the radical pair is formed by a Chl donor and a Phe acceptor having well separated signals (Fig. 4B) (Table 2). The donor signals were remarkably narrow (full width at half-height, FWHH, of ~40 Hz), whereas the acceptor signals were slightly broader (~70 Hz) implying a general feature of photosynthetic RCs having a rigid donor site without structural heterogeneities [13,71] and slightly more structural flexibility at the acceptor site. The intensity ratio of light induced signals from the Chl donor cofactor shows a strong asymmetry of electron spin density, which appears to be shifted toward the pyrrole ring IV (Fig. 4C). These observations were in line with the strong asymmetry of electron spin density detected previously by ^{13}C photo-CIDNP MAS NMR demonstrating maximum electron spin density at the neighboring C-15 methine carbon [53]. Thus, the electron spin density pattern is inverted in the donor of PSII as compared with the donor and acceptor cofactors in PSI, as well as to isolated Chl *a* cofactors. On the other hand, there was no indication for a significant disturbance of the electronic ground state (chemical shifts) and the change in the electronic structure was found to be restricted to the photo-oxidized state (signal intensities).

Interestingly, ^{15}N photo-CIDNP spectra of PSII RC also showed a comparably broad signal at 243.8 ppm which was proposed to be arising from the structurally more a flexible unit close to the donor Chl (Fig. 4B) [54]. This signal was assigned to the N-π of a type-1 histidine (i.e., carrying a lone pair at the π-position [13]). ^{13}C photo-CIDNP MAS NMR of PSII RC also show signals arising from a histidine assumable in the close proximity to the Chl donor. The ^{13}C signals assigned to a histidine show another orientation dependence than the Chl cofactor [54]. It was therefore proposed that the electron spin density is distributed over both the donor Chl and its axial histidine. These results were in line with EPR studies which show only 82% spin density on one Chl cofactor. The photo-CIDNP studies imply that the remaining spin density is localized on the axial histidine. Hence, the donor must be an inner Chl, either P_{D1} or P_{D2}, because the two accessory Chls, Chl_{D1} and Chl_{D2}, are not coordinated to histidines.

5.3. The hinge model of the electron donor in PSII

Based on both ^{13}C and ^{15}N photo-CIDNP MAS NMR results, Diller et al. [54] proposed the "hinge model" for the donor complex of PSII (Fig. 4D). Here, the electron spin density is proposed to be shared between the donor Chl and its axial histidine being tilted toward the pyrrole ring IV and the C-15 methine bridge. Since the accessory chlorophylls Chl_D are not coordinated to a histidine residue [30], the donor candidate was proposed to be an inner chlorophyll. This is in line with EPR studies proposing P_D as the donor on the time-scale of magnetic resonance experiments [74,75]. A model of π-deprotonated type-1 histidine [76] would generate a donor complex $[Chl\text{-}His]^-$ which, upon photo-oxidation, is transformed from a negatively charged ground state donor to a neutral radical. The proposed explanation was in agreement with preliminary density functional computations suggesting that a minor tilt could result in both a spin density shift toward pyrrole ring-IV as well as on the histidine amino acid [54]. Thus, the hinge model of the electron donor in PSII in principle explains the observed inversion of the pattern of electron spin density distribution on the donor Chl.

6. Magnetic field effect of the photo-CIDNP observed in photosystem I and II reaction centers

Photo-CIDNP effects in liquid and solid state show strong magnetic field dependence which is indicative for the mechanisms and the parameters causing the effect [60,64,77–79]. Interestingly, the solid-state photo-CIDNP effects observed in PSI and PSII exhibit very different magnetic field dependencies (Fig. 5). For PSI, the maximum photo-CIDNP enhancement is observed at 9.4 T [51], while the strongest signal enhancement for PSII has been observed at 4.7 T. It is still not clear whether a lower magnetic field would improve the signal enhancement for PSII further. In RCs of *R. sphaeroides* R26, the strongest effect, in particular for the DR, was observed at 1.4 T [40,48]. The field dependence of PSI CIDNP shows similarities to the field dependence observed for RC from heliobacteria [69]. Both PSI and heliobacterial RC are Type I RCs. On the other hand, the field dependence of PSII shows similarities to that observed in RCs of *R. sphaeroides* [40]. Both *R. sphaeroides* RC and

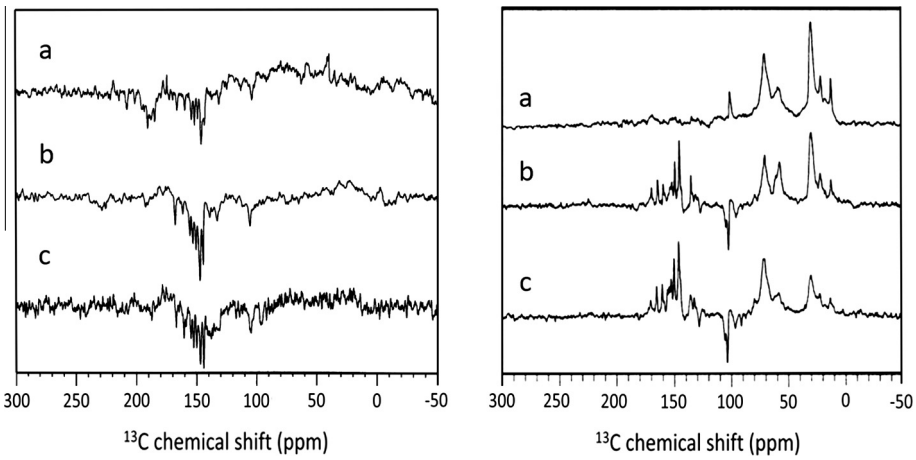

Fig. 5. Magnetic field dependence of ^{13}C photo-CIDNP MAS NMR spectra of natural abundance PSI (left) and PSII (right) of spinach. Spectra were recorded under continuous illumination with white light at three different magnetic fields, (a) 17.6, (b) 9.4 T and (c) 4.7 T at 8 kHz MAS frequency. Reprinted, with permission, from Roy et al. [51]. © Springer.

PSII are Type II RCs. It is possible that the magnetic field dependence of the photo-CIDNP effect is due to the difference between Type I and Type II RCs. The difference might reflect differences in coupling between the free electrons on the donor and acceptor site during the radical pair state.

7. Summary and outlook

Photo-CIDNP MAS NMR became complementary to the existing spectroscopic tool box. It provides information on electronic structures as the EPR family of methods does, however with atomic resolution. Compared to EPR, it also provides access to the diamagnetic ground state. While the ^{1}H electron nuclear double resonance (ENDOR) methods probe the s spin densities mainly for nuclei outside the ring, ^{13}C photo-CIDNP MAS NMR is correlated to the p_z electron spin density in the radical pair state. Therefore, photo-CIDNP MAS NMR is a unique tool to provide a coherent molecular picture of the unpaired electron density distribution in the radical pair with atomic selectivity in a single experiment. Photo-CIDNP MAS NMR has a lower temporal resolution than optical spectroscopy [80]. It provides kinetic information on the microsecond timescale, however it provides access to local electronic effects. Furthermore, the method can be used to explore structural details such as distance information and hydrogen bonding interactions and therefore it can be complementary to X-ray crystallography. Hence, photo-CIDNP MAS NMR has emerged as a fully-fledged analytical method for studying systems that carry spin-correlated radical pairs. In natural photosynthesis and other light-induced electron transfer chains, spin-correlated radical pair species frequently occur, making this field the ideal ground to evolve this method.

A major limitation toward the progress in investigating PSI and PSII in plants, algae and cyanobacteria by MAS NMR has so far been the lack of methods to introduce sufficient isotope labeling for obtaining higher selectivity and sensitivity and to get sufficient amounts of labeled material to prepare pure RC. However, recent advances suggest that these limitations can be overcome and the primary charge separation and electron transfer events can be investigated in PSI and PSII in whole cells using photo-CIDNP MAS NMR [54–56,70]. Subsequently, the search for new organisms showing the solid-state photo-CIDNP effect is no longer constrained by the isolation procedure. Several important issues have been partially resolved using photo-CIDNP MAS NMR methods. For example, the matrix involvement in tuning the donor of PSII, the asymmetry of monomeric donor and the remarkable differences in the electronic structures of the donors of PSI and PSII.

Acknowledgements

The authors thank Prof. Gunnar Jeschke for exciting discussions. The financial support from NWO grant (713.012.001), FOM grant (10TBSC23) and DFG grant (MA 4972/2-1) is gratefully acknowledged. M. Najdanova thanks German Academic Exchange Service (DAAD) for a research fellowship.

References

[1] R.E. Blankenship, Molecular Mechanisms of Photosynthesis, Blackwell Science, Oxford, 2002.
[2] A.W. Rutherford, P. Heathcote, Primary photochemistry in photosystem-I, Photosynth. Res. 6 (1985) 295–316.
[3] Y. Mazor, A. Borovikova, N. Nelson, The structure of plant photosystem I supercomplex at 2.8 Å resolution, eLife 4 (2015).
[4] A. Amunts, H. Toporik, A. Borovikova, N. Nelson, Structure determination and improved model of plant photosystem I, J. Biol. Chem. 285 (2010) 3478–3486.
[5] W. Saenger, P. Jordan, N. Krauss, The assembly of protein subunits and cofactors in photosystem I, Curr. Opin. Struct. Biol. 12 (2002) 244–254.
[6] S.P. Romberger, J.H. Golbeck, The bound iron-sulfur clusters of type-I homodimeric reaction centers, Photosynth. Res. 104 (2010) 333–346.
[7] T. Watanabe, M. Kobayashi, A. Hongu, M. Nakazato, T. Hiyama, N. Murata, Evidence that a chlorophyll a' dimer constitutes the photochemical reaction centre 1 (P700) in photosynthetic apparatus, FEBS Lett. 191 (1985) 252–256.
[8] P. Jordan, P. Fromme, H.T. Witt, O. Klukas, W. Saenger, N. Krauss, Three-dimensional structure of cyanobacterial photosystem I at 2.5 Å resolution, Nature 411 (2001) 909–917.
[9] A.N. Webber, W. Lubitz, P700: the primary electron donor of photosystem I, Biochim. Biophys. Acta 1507 (2001) 61–79.
[10] A.R. Holzwarth, M.G. Müller, J. Niklas, W. Lubitz, Ultrafast transient absorption studies on photosystem I reaction centers from *Chlamydomonas reinhardtii*. 2: mutations near the P700 reaction center chlorophylls provide new insight into the nature of the primary electron donor, Biophys. J. 90 (2006) 552–565.
[11] H. Käss, P. Fromme, H.T. Witt, W. Lubitz, Orientation and electronic structure of the primary donor radical cation in photosystem I: a single crystals EPR and ENDOR study, J. Phys. Chem. B 105 (2001) 1225–1239.
[12] H. Käss, E. Bittersmann-Weidlich, L.-E. Andréasson, B. Bönigk, W. Lubitz, ENDOR and ESEEM of the 15N labelled radical cations of chlorophyll a and the primary donor P700 in photosystem I, Chem. Phys. 194 (1995) 419–432.
[13] Alia, E. Roy, P. Gast, H.J. van Gorkom, H.J.M. de Groot, G. Jeschke, J. Matysik, Photochemically induced dynamic nuclear polarization in photosystem I of plants observed by 13C magic-angle spinning NMR, J. Am. Chem. Soc. 126 (2004) 12819–12826.
[14] S. Santabarbara, L. Galuppini, A.P. Casazza, Bidirectional electron transfer in the reaction centre of photosystem I, J. Integr. Plant. Biol. 52 (2010) 735–749.
[15] M.G. Müller, J. Niklas, W. Lubitz, A.R. Holzwarth, Ultrafast transient absorption studies on Photosystem I reaction centers from *Chlamydomonas reinhardtii*. 1. A new interpretation of the energy trapping and early electron transfer steps in Photosystem I, Biophys. J. 85 (2003) 3899–3922.

[16] M.G. Müller, C. Slavov, R. Luthra, K.E. Redding, A.R. Holzwarth, Independent initiation of primary electron transfer in the two branches of the photosystem I reaction center, Proc. Natl Acad. Sci. USA 107 (2010) 4123–4128.
[17] S. Santabarbara, P. Heathcote, M.C.W. Evans, Modelling of the electron transfer reactions in Photosystem I by electron tunnelling theory: the phylloquinones bound to the PsaA and the PsaB reaction centre subunits of PS I are almost isoenergetic to the iron–sulfur cluster F(X), Biochim. Biophys. Acta 1708 (2005) 283–310.
[18] N. Srinivasan, J.H. Golbeck, Protein–cofactor interactions in bioenergetic complexes: the role of the A1A and A1B phylloquinones in Photosystem I, Biochim. Biophys. Acta 1787 (2009) 1057–1088.
[19] H.T. Witt, Energy conversion in the functional membrane of photosynthesis. Analysis by light pulse and electric pulse methods, Biochim. Biophys. Acta 505 (1979) 355–427.
[20] A. Hope, Electron transfers amongst cytochrome f, plastocyanin and photosystem I: kinetics and mechanisms, Biochim. Biophys. Acta. 1456 (2000) 5–26.
[21] W.V. Fairclough, A. Forsyth, M.C.W. Evans, S.E.J. Rigby, S. Purton, P. Heathcote, Bidirectional electron transfer in photosystem I: electron transfer on the PsaA side is not essential for phototrophic growth in Chlamydomonas, Biochim. Biophys. Acta 1606 (2003) 43–55.
[22] L. Krabben, E. Schlodder, R. Jordan, D. Carbonera, G. Giacometti, H. Lee, A.N. Webber, W. Lubitz, Influence of the axial ligands on the spectral properties of P700 of Photosystem I: a study of site-directed mutants, Biochemistry 39 (2000) 13012–13025.
[23] R.O. Cohen, G. Shen, J.H. Golbeck, W. Xu, P.R. Chitnis, A.I. Valieva, A. van der Est, Y. Pushkar, D. Stehlik, Evidence for asymmetric electron transfer in cyanobacterial photosystem I: analysis of a methionine-to-leucine mutation of the ligand to the primary electron acceptor A0, Biochemistry 43 (2004) 4741–4754.
[24] F. Rappaport, B.A. Diner, K. Redding, Optical measurements of secondary electron transfer in Photosystem I, in: J.H. Golbeck (Ed.), Photosystem I, Springer, Netherlands, Dordrecht, 2006, pp. 223–244.
[25] Y. Li, A. van der Est, M.G. Lucas, V.M. Ramesh, F. Gu, A. Petrenko, S. Lin, A.N. Webber, F. Rappaport, K. Redding, Directing electron transfer within Photosystem I by breaking H-bonds in the cofactor branches, Proc. Natl. Acad. Sci. USA 103 (2006) 2144–2149.
[26] V.M. Ramesh, K. Gibasiewicz, S. Lin, S.E. Bingham, A.N. Webber, Bidirectional electron transfer in Photosystem I: accumulation of A 0- in A-side or B-side mutants of the axial ligand to Chlorophyll A 0, Biochemistry 43 (2004) 1369–1375.
[27] N. Dashdorj, W. Xu, R.O. Cohen, J.H. Golbeck, S. Savikhin, Asymmetric electron transfer in cyanobacterial Photosystem I: charge separation and secondary electron transfer dynamics of mutations near the primary electron acceptor A0, Biophys. J. 88 (2005) 1238–1249.
[28] Y. Umena, K. Kawakami, J.R. Shen, N. Kamiya, Crystal structure of oxygen-evolving photosystem II at a resolution of 1.9 Å, Nature 473 (2011) 55–60.
[29] N. Kamiya, J.R. Shen, Crystal structure of oxygen-evolving photosystem II from *Thermosynechococcus vulcanus* at 3.7-Å resolution, Proc. Natl. Acad. Sci. USA 100 (2003) 98–103.
[30] A. Zouni, H.T. Witt, J. Kern, P. Fromme, N. Krauss, W. Saenger, P. Orth, Crystal structure of photosystem II from *Synechococcus elongatus* at 3.8 Å resolution, Nature 409 (2001) 739–743.
[31] K.N. Ferreira, T.M. Iverson, K. Maghlaoui, J. Barber, S. Iwata, Architecture of the photosynthetic oxygen-evolving center, Science (New York, N.Y.) 303 (2004) 1831–1838.
[32] B.A. Diner, E. Schlodder, P.J. Nixon, W.J. Coleman, F. Rappaport, J. Lavergne, W. F. Vermaas, D.A. Chisholm, Site-directed mutations at D1-His198 and D2-His197 of photosystem II in Synechocystis PCC 6803: sites of primary charge separation and cation and triplet stabilization, Biochemistry 40 (2001) 9265–9281.
[33] B.A. Diner, F. Rappaport, Structure, dynamics, and energetics of the primary photochemistry of photosystem II of oxygenic photosynthesis, Annu. Rev. Plant. Biol. 53 (2002) 551–580.
[34] S. Caffarri, T. Tibiletti, R.C. Jennings, S. Santabarbara, A comparison between plant photosystem I and photosystem II architecture and functioning, Curr. Protein. Pept. Sci. 15 (2014) 296–331.
[35] V.I. Novoderezhkin, E. Romero, J.P. Dekker, R. van Grondelle, Multiple charge-separation pathways in photosystem II: modeling of transient absorption kinetics, ChemPhysChem 12 (2011) 681–688.
[36] H.J. van Gorkom, J.P. Schelvis, Kok's oxygen clock: what makes it tick? The structure of P680 and consequences of its oxidizing power, Photosynth. Res. 38 (1993) 297–301.
[37] Alia, B. Hulsebosch, H.J. van Gorkom, J. Raap, J. Lugtenburg, J. Matysik, H.J.M. de Groot, P. Gast, Probing the electronic structure of tyrosine radical YD in photosystem II by EPR spectroscopy using site specific isotope labelling in *Spirodela oligorrhiza*, Chem. Phys. 294 (2003) 459–469.
[38] X. Lin, H.A. Murchison, V. Nagarajan, W.W. Parson, J.P. Allen, J.C. Williams, Specific alteration of the oxidation potential of the electron donor in reaction centers from *Rhodobacter sphaeroides*, Proc. Natl. Acad. Sci. USA 91 (1994) 10265–10269.
[39] E. Daviso, A. Alia, S. Prakash, A. Diller, P. Gast, J. Lugtenburg, J. Matysik, G. Jeschke, Electron–nuclear spin dynamics in a bacterial photosynthetic reaction center, J. Phys. Chem. C 113 (2009) 10269–10278.
[40] S.S. Thamarath, B.E. Bode, S. Prakash, K.B.S.S. Gupta, Alia, G. Jeschke, J. Matysik, Electron spin density distribution in the special pair triplet of *Rhodobacter sphaeroides* R26 revealed by magnetic field dependence of the solid-state photo-CIDNP effect, J. Am. Chem. Soc. 134 (2012) 5921–5930.
[41] J. Bargon, H. Fischer, U. Johnson, Kernresonanz-Emissionslinien während rascher Radikalreaktionen. 1. Aufnahmeverfahren und Beispiele, Z., Naturforsch. A (1967) 1551–1562.
[42] H.R. Ward, R.G. Lawler, Nuclear magnetic resonance emission and enhanced absorption in rapid organometallic reactions, J. Am. Chem. Soc. 89 (1967) 5518–5519.
[43] G.L. Closs, L.E. Closs, Induced dynamic nuclear spin polarization in reactions of photochemically and thermally generated triplet diphenylmethylene, J. Am. Chem. Soc. 91 (1969) 4549–4550.
[44] R. Kaptein, J.L. Oosterhoff, Chemically induced dynamic nuclear polarization II, Chem. Phys. Lett. 4 (1969) 195–197.
[45] G. Jeschke, J. Matysik, A reassessment of the origin of photochemically induced dynamic nuclear polarization effects in solids, Chem. Phys. 294 (2003) 239–255.
[46] M.G. Zysmilich, A. McDermott, Photochemically induced dynamic nuclear polarization in the solid-state 15N spectra of reaction centers from photosynthetic bacteria *Rhodobacter sphaeroides* R-26, J. Am. Chem. Soc. 116 (1994) 8362–8363.
[47] Govindjee, T.J. Aartsma, J. Matysik (Eds.), Biophysical Techniques in Photosynthesis, Springer, Netherlands, Dordrecht, 2008.
[48] S. Prakash, Alia, P. Gast, H.J.M. de Groot, G. Jeschke, J. Matysik, Magnetic field dependence of photo-CIDNP MAS NMR on photosynthetic reaction centers of *Rhodobacter sphaeroides* WT, J. Am. Chem. Soc. 127 (2005) 14290–14298.
[49] S. Prakash, Alia, P. Gast, H.J.M. de Groot, J. Matysik, G. Jeschke, Photo-CIDNP MAS NMR in intact cells of *Rhodobacter sphaeroides* R26: molecular and atomic resolution at nanomolar concentration, J. Am. Chem. Soc. 128 (2006) 12794–12799.
[50] J.F. Allen, E. Gantt, J.H. Golbeck, B. Osmond (Eds.), Photosynthesis. Energy from the Sun, Springer, Netherlands, Dordrecht, 2008.
[51] E. Roy, Alia, P. Gast, H. van Gorkom, H.J.M. de Groot, G. Jeschke, J. Matysik, Photochemically induced dynamic nuclear polarization in the reaction center of the green sulphur bacterium *Chlorobium tepidum* observed by 13C MAS NMR, Biochim. Biophys. Acta 1767 (2007) 610–615.
[52] E. Roy, T. Rohmer, P. Gast, G. Jeschke, Alia, J. Matysik, Characterization of the primary radical pair in reaction centers of *Heliobacillus mobilis* by 13C photo-CIDNP MAS NMR, Biochemistry 47 (2008) 4629–4635.
[53] J. Matysik, Alia, P. Gast, H.J. van Gorkom, A.J. Hoff, H.J. de Groot, Photochemically induced nuclear spin polarization in reaction centers of photosystem II observed by 13C-solid-state NMR reveals a strongly asymmetric electronic structure of the P680(.+) primary donor chlorophyll, Proc. Natl Acad. Sci. USA 97 (2000) 9865–9870.
[54] A. Diller, E. Roy, P. Gast, H.J. Van Gorkom, H.J.M. de Groot, C. Glaubitz, G. Jeschke, J. Matysik, Alia, 15N photochemically induced dynamic nuclear polarization magic-angle spinning NMR analysis of the electron donor of photosystem II, Proc. Natl Acad. Sci. USA 104 (2007) 12767–12771.
[55] G.J. Janssen, E. Daviso, M. van Son, H.J.M. de Groot, Alia, J. Matysik, Observation of the solid-state photo-CIDNP effect in entire cells of cyanobacteria Synechocystis, Photosynth. Res. 104 (2010) 275–282.
[56] G.J. Janssen, E. Roy, J. Matysik, Alia, 15N photo-CIDNP MAS NMR to reveal functional heterogeneity in electron donor of different plant organisms, Appl. Magn. Reson. 42 (2012) 57–67.
[57] J. Golbeck, A. van der Est (Eds.), The Biophysics of Photosynthesis, Springer, New York, NY, 2014.
[58] G. Jeschke, Electron–electron–nuclear three-spin mixing in spin-correlated radical pairs, J. Chem. Phys. 106 (1997) 10072–10086.
[59] G. Jeschke, A new mechanism for chemically induced dynamic nuclear polarization in the solid state, J. Am. Chem. Soc. 120 (1998) 4425–4429.
[60] J. Matysik, A. Diller, E. Roy, Alia, The solid-state photo-CIDNP effect, Photosynth. Res. 102 (2009) 427–435.
[61] R. Kaptein, Simple rules for chemically induced dynamic nuclear polarization, J. Chem. Soc. D (1971) 732–733.
[62] R.A. Goldstein, S.G. Boxer, Effect of nuclear-spin polarization on the reaction dynamics in photosynthetic bacterial reaction centers, Biophys. J. 51 (1987) 937–946.
[63] A. McDermott, M.G. Zysmilich, T. Polenova, Solid state NMR studies of photoinduced polarization in photosynthetic reaction centers: mechanism and simulations, Solid State Nucl. Magn. Reson. 11 (1998) 21–47.
[64] B.E. Bode, S.S. Thamarath, K.B.S.S. Gupta, Alia, G. Jeschke, J. Matysik, The solid-state photo-CIDNP effect and its analytical application, in: L.T. Kuhn (Ed.), Hyperpolarization Methods in NMR Spectroscopy, Springer, Berlin, Heidelberg, 2013, pp. 105–121.
[65] E. Daviso, G. Jeschke, J. Matysik, Photochemically induced dynamic nuclear polarization (photo-CIDNP) magic-angle spinning NMR, in: Govindjee, T.J. Aartsma, J. Matysik (Eds.), Biophysical Techniques in Photosynthesis, Springer, Netherlands, Dordrecht, 2008, pp. 385–399.
[66] I.F. Céspedes-Camacho, J. Matysik, Spin in photosynthetic electron transport, in: J. Golbeck, A. van der Est (Eds.), The Biophysics of Photosynthesis, Springer, New York, NY, 2014, pp. 141–170.
[67] G. Jeschke, B.C. Anger, B.E. Bode, J. Matysik, Theory of solid-state photo-CIDNP in the earth's magnetic field, J. Phys. Chem. A 115 (2011) 9919–9928.

[68] E. Daviso, G.J. Janssen, Alia, G. Jeschke, J. Matysik, M. Tessari, A 10000-fold nuclear hyperpolarization of a membrane protein in the liquid phase via a solid-state mechanism, J. Am. Chem. Soc. 133 (2011) 16754–16757.
[69] S.S. Thamarath, Alia, E. Roy, K.B.S.S. Gupta, J.H. Golbeck, J. Matysik, The field-dependence of the solid-state photo-CIDNP effect in two states of heliobacterial reaction centers, Photosynth. Res. 117 (2013) 461–469.
[70] A. Diller, Alia, E. Roy, P. Gast, H.J. vanGorkom, J. Zaanen, H.J.M. deGroot, C. Glaubitz, J. Matysik, Photo-CIDNP solid-state NMR on Photosystems I and II: what makes P680 special?, Photosynth Res. 84 (2005) 303–308.
[71] M.R. Fischer, H.J.M. deGroot, J. Raap, C. Winkel, A.J. Hoff, J. Lugtenburg, Carbon-13 magic angle spinning NMR study of the light-induced and temperature-dependent changes in *Rhodobacter sphaeroides* R26 reaction centers enriched in [4′-13C]tyrosine, Biochemistry 31 (1992) 11038–11049.
[72] S. Prakash, Alia, P. Gast, G. Jeschke, H.J.M. deGroot, J. Matysik, Photochemically induced dynamic nuclear polarisation in entire bacterial photosynthetic units observed by 13C magic-angle spinning NMR, J. Mol. Struct. 661–662 (2003) 625–633.
[73] M. Rögner, P.J. Nixon, B.A. Diner, Purification and characterization of photosystem I and photosystem II core complexes from wild-type and phycocyanin-deficient strains of the cyanobacterium Synechocystis PCC 6803, J. Biol. Chem. 265 (1990) 6189–6196.
[74] W. Lubitz, F. Lendzian, R. Bittl, Radicals, radical pairs and triplet states in photosynthesis, Acc. Chem. Res. 35 (2002) 313–320.
[75] S.G. Zech, J. Kurreck, H.J. Eckert, G. Renger, W. Lubitz, R. Bittl, Pulsed EPR measurement of the distance between P680+.·and QA−.·in photosystem II, FEBS Lett. 414 (1997) 454–456.
[76] Alia, J. Matysik, C. Soede-Huijbregts, M. Baldus, J. Raap, J. Lugtenburg, P. Gast, H.J. van Gorkom, A.J. Hoff, H.J. de Groot, Ultrahigh field MAS NMR dipolar correlation spectroscopy of the histidine residues in light-harvesting complex II from photosynthetic bacteria reveals partial internal charge transfer in the B850/His complex, J. Am. Chem. Soc. 123 (2001) 4803–4809.
[77] C.B. Grissom, Magnetic field effects in biology: a survey of possible mechanisms with emphasis on radical-pair recombination, Chem. Rev. 95 (1995) 3–24.
[78] A.J. Hoff, Magnetic field effects on photosynthetic reactions, Quart. Rev. Biophys. 14 (1981) 599–665.
[79] S.G. Boxer, C.E.D. Chidsey, M.G. Roelofs, Magnetic field effects on reaction yields in the solid state: an example from photosynthetic reaction centers, Annu. Rev. Phys. Chem. 34 (1983) 389–417.
[80] E. Schlodder, Introduction to optical methods in photosynthesis, Photosynth. Res. 101 (2009) 93–104.